Chemosphere 305 (2022) 135481

Contents lists available at ScienceDirect

Chemosphere

journal homepage: www.elsevier.com/locate/chemosphere

PM_{10} prediction for brake wear of passenger car during different test driving cycles

Ye Liu [a,*], Haibo Chen [a,**], Chuhan Yin [a], Matteo Federici [b], Guido Perricone [b], Ying Li [c], Dimitris Margaritis [d], Yang Shen [e], Junhua Guo [f], Tangjian Wei [a,f]

[a] Institute for Transport Studies, University of Leeds, Leeds, LS2 9JT, UK
[b] Brembo S.p.A., Via Europa 2, 24020, Stezzano (BG), Italy
[c] Dynnoteq, 61 Bridge Street, Kington, HR5 3DJ, UK
[d] Centre for Research and Technology Hellas (CERTH), Hellenic Institute of Transport (HIT), 6th km Charilaou-Thermi, 57001, Thermi, Thessaloniki, Greece
[e] Zhejiang Xinchai CO., LTD, Shaoxin, 312500, China
[f] School of Transportation Engineering, East China Jiaotong University, Jiangxi, 330013, China

HIGHLIGHTS

- Brake wear PM_{10} emissions under three test driving cycles were studies using FEA.
- PM_{10} emissions were measured on a brake dynamometer to validate FEA approach.
- PM_{10} EFs under the WLTP, LACT, WLTP-Brake were 7.9, 9.8, and 6.4 mg km^{-1} veh^{-1}.
- PM_{10} EFs showed a greater fraction of total mass EFs in LACT than other two cycles.

GRAPHICAL ABSTRACT

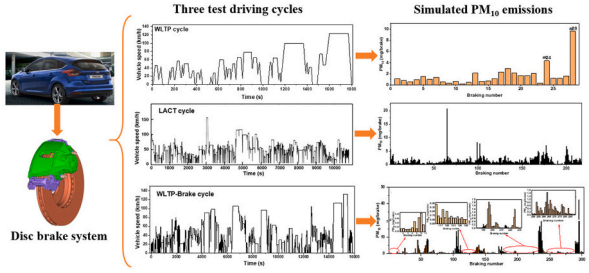

ARTICLE INFO

Handling Editor: Derek Muir

Keywords:
Air quality
Non-exhaust emissions
Brake wear
PM_{10} emissions
FEA

ABSTRACT

PM_{10} emissions generated from the brake wear of passenger car per braking event during three test driving cycles (WLTP, LACT, and WLTP-Brake) were studied using a finite element analysis (FEA) approach in combination with the relationship among the mass emitted rate of airborne particles versus local contact pressure and sliding speed. In addition, PM_{10} emissions were measured per braking event during the WLTP-Brake cycle on a brake dynamometer using an electrical low-pressure impactor (ELPI+) to validate the proposed FEA approach. The simulated and experimental results for WLTP-Brake illustrated that the proposed simulation approach has the potential to predict PM_{10} from brake wear per braking event, with an R^2 value of 0.93. The FEA results of three test driving cycles showed that there was a gradient rise in pad wear on both sides from the inner to outer radii. The simulated PM_{10} emission factors during the WLTP, LACT, and WLTP-Brake were 7.9 mg km^{-1} veh^{-1}, 9.8 mg km^{-1} veh^{-1}, and 6.4 mg km^{-1} veh^{-1}, respectively. Among three test driving cycles, the ratio of PM_{10} to total brake wear mass per braking event was the largest for the LACT, followed by WLTP and WLTP-Brake. From a practical application perspective, reducing the frequency of high-speed braking may be an effective way to decrease the generation of PM_{10} emissions.

* Corresponding author.
** Corresponding author.
E-mail addresses: Y.Liu8@leeds.ac.uk (Y. Liu), H.Chen@its.leeds.ac.uk (H. Chen).

https://doi.org/10.1016/j.chemosphere.2022.135481
Received 15 April 2022; Received in revised form 1 June 2022; Accepted 21 June 2022
Available online 23 June 2022

1. Introduction

Non-exhaust particulate matter (PM) emissions, including brake wear, tyre wear, road wear, and resuspension of road dust, are a major problem for the air quality in cities due to the effects on the environment and human health (Klöckner et al., 2021; Woo et al., 2021; Zhang et al., 2018). Previous studies have demonstrated that non-exhaust PM emissions are comparable to or even more than the vehicle exhaust PM_{10} emissions and that their relative contribution to the total vehicle PM emissions is increasing as a better understanding of the generation mechanism and physicochemical properties of PM improves the development of combustion control and after-treatment technologies, and thus vehicle exhaust PM is reduced significantly (Liu et al., 2016, 2022b; Pant and Harrison, 2013; Zhang et al., 2021). The non-exhaust PM emissions, however, have long been neglected. Amongst these non-exhaust PM emissions, brake wear PM emissions are particularly significant since these particles are far smaller than others of the non-exhaust emissions, and hazardous metals are frequently discovered in brake wear particles (Contardo et al., 2020; Grigoratos and Martini, 2015; Shupert et al., 2013). In addition, brake wear PM is the main contributor to non-exhaust PM emissions. For instance, Harrison et al. (2012) revealed that brake wear particles contributed up to 55% by weight to of total non-exhaust emissions and it was evaluated that as much as 50% of brake wear particles would become airborne, with 80–98% of these particles falling into the PM_{10} range (Hagino et al., 2015). It was found that 21% of total road-traffic related PM_{10} emissions resulted from brake wear particles (Gasser et al., 2009; Lawrence et al., 2013). Brake and tyre wear particles accounted for 34% of the traffic-related PM_{10} in the report of the European Environment Agency (EEA, 2018). Thus, further investigation is needed to obtain a better understanding of the generation mechanism of brake wear particles.

The brake wear particles are highly dependent on the distributions of contact pressure and sliding velocity at the contact surface between the brake rotor and pads (Kukutschová et al., 2011; Sanders et al., 2003; Wahlström et al., 2017). In terms of the experimental method, it is difficult to investigate the real-time changes in the contact pressure and sliding velocity between them. Thus, in order to explore what is taking place at the contact surface of the brake pad and disc during braking, several simulation approaches were developed by different researchers. For instance, AbuBakar and Ouyang (2008) evaluated the contact pressure between brake pads and rotor using a finite element analysis (FEA) approach and performed a comparative analysis with the experimental results. Schmidt et al. (2018) carried out a wear analysis on a tilted shaft-bushing bearing using a transient non-linear FEA. Recently, Riva et al. (2019) developed the FEA approach to predict airborne particle emissions of the Los Angeles City traffic cycle (LACT). Moreover, Riva et al. (2020) determined the overall coefficient of friction for a disc brake system using an FEA approach in conjunction with a *pv*-map coefficient of friction. To the best of our knowledge, however, there is limited information about the use of the FEA approach to evaluate brake wear airborne particles, particularly throughout various test-driving cycles. The simulation work is able to explain physical phenomena that occur during experiments and evaluate how a novel design of brake system will work during operation. In addition, the FEA approach can provide a simulation of wear and airborne emissions from disc brakes, which is an essential tool during the design phase of innovative disc brake systems with low emissions.

In this context, an FEA approach in the present work was used to explore the brake pad contact pressure and wear depth distributions for each braking event during the worldwide harmonised light-duty vehicle test procedure (WLTP), LACT, and the world harmonised light-duty vehicle test procedure-brake (WLTP-Brake) cycle. In addition, the PM_{10} emissions from brake wear were computed using an EFA and measured on a brake dynamometer to validate this FEA approach.

2. Simulation methodology and validation

2.1. Simulation methodology

A schematic representation of the FEA approach is illustrated in Fig. 1. To begin, a three-dimensional model was built, specifying the material qualities of various components, and configuring the driving conditions. The *pv*-map of the local particle rate against sliding velocity and normal contact pressure, obtained from tribometer testing (Wahlström et al., 2017) was used as input data to forecast brake wear emissions. Simultaneously, the brake wear PM_{10} emissions per brake were measured throughout the WLTP-Brake cycle on a brake dynamometer. Lastly, following post-processing activities, a comparison of the measured and simulated results was performed to validate the proposed FEA simulation approach.

2.1.1. Finite element analysis (FEA)

A medium-sized car's left front disc braking system was chosen for the present study, as illustrated in Fig. 2. This brake system includes a carrier, a floating calliper, a rotor made of grey cast iron, two pads, a piston, and two sliding pins with two bushings. The inner and outer radii of the rotor ring are 80 mm and 139 mm, as well as the piston diameter and pad surface area are 57 mm and 5080 mm^2 (Riva et al., 2019).

The commercial software ABAQUS was used to perform finite element analysis (ABAQUS, 2014). Fig. 3 depicts the disc brake system after the components have been meshed. The tetrahedral mesh was employed to construct the carrier, floating calliper, and piston head, and the hexahedral mesh was used to build the remaining components. The mesh size ranges from 2 mm to 8 mm, with a mean value of 4 mm. The applied pressure and rotational speed were determined according to the braking characteristics of each braking event during three test driving cycles, which were applied to the piston head and rotor, respectively. In terms of each braking event throughout three test driving cycles, a quasi-static FEA was conducted to compute the contact pressure and slip rate of each node and element of the brake pads at each step of the

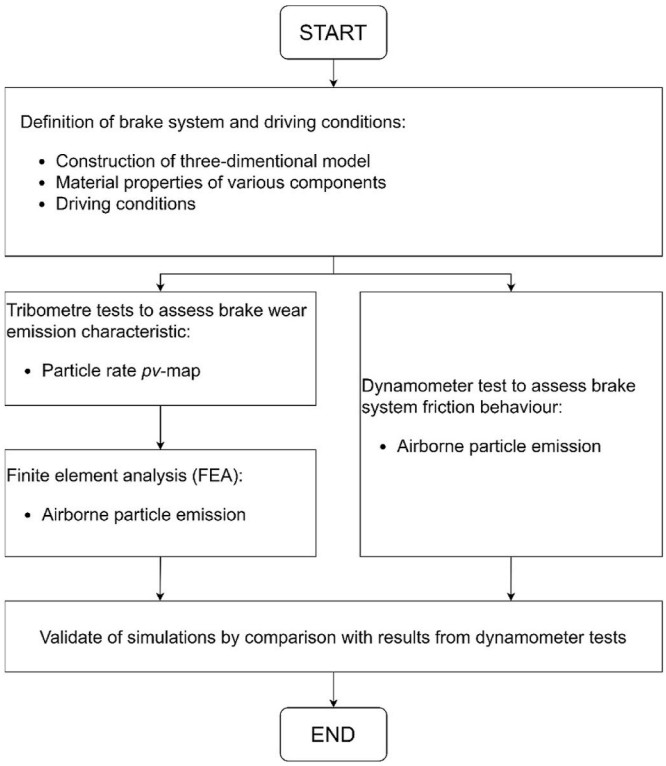

Fig. 1. A schematic representation of the FEA approach.

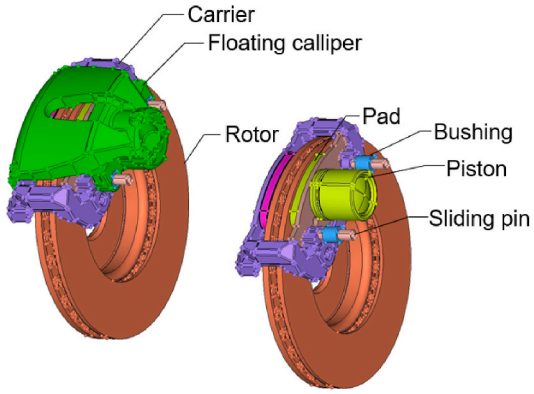

Fig. 2. Disc brake system with a single piston.

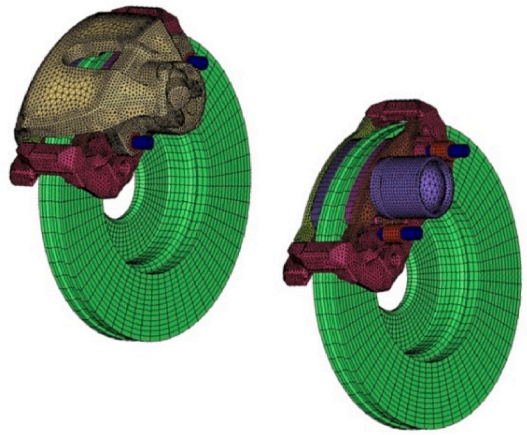

Fig. 3. Mesh of the disc brake system.

braking event. After each step, the node coordinates were updated using the Abaqus Arbitrary Lagrangian-Eulerian adaptive meshing approach (Abaqus).

2.1.2. Brake cases

Three typical test driving cycles, that is, WLTP, LACT, and WLTP-Brake, were used in the current work to investigate the brake wear PM_{10} emissions. The WLTP was a recently developed test driving cycle for measuring vehicle exhaust pollutant emissions (Tutuianu et al., 2015), which reflected the average driving pattern of light-duty vehicles, according to 700,000 vehicle driving data from Europe, the United States, India, Korea, and Japan. The WLTP was simplified based on the methods proposed by Mathissen et al. (2018) and Park et al. (2021). The simplified WLTP consisted of 28 braking events where the average braking speed and a deceleration rate were 32.5 km/h and 0.94 m/s^2, respectively. The LACT was designed to measure brake wear particles under urban driving conditions. The LACT was developed by Mathissen and Evans (2019), where the median initial speed and deceleration rates were kept the same as the full LACT. This cycle lasted 180 min, covered 150 km, and had an average braking speed of 36.7 km/h and a mean deceleration rate of 1.07 m/s^2. The WLTP-Brake was designed to measure brake wear particles according to the vehicle driving data of the WLTP, which included 303 braking events. The braking deceleration rates ranged from 0.49 to 2.18 m/s^2 with an average value of 0.97 m/s^2, and the average braking speed was 43.7 km/h.

2.1.3. PM_{10} emission computation

The *pv*-map of airborne particle mass rate versus sliding speed and normal contact pressure was obtained by Wahlström et al. (2017) in the pin-on-disc experiments, as shown in Fig. 4. This *pv*-map was employed as input data in the present work to compute brake wear particles. The particle emission per sliding distance (μg/m) was able to be obtained from this *pv*-map based on the known node contact pressure and sliding velocity. Considering that deceleration rate and contact pressure during each braking event were considered to remain constant, each braking event could be divided into *n* sub-steps. The PM_{10} mass for each element of every braking event was calculated from the following equations (Riva et al., 2019):

$$m_{particle} = \varphi_{POD}\left(\sum_{i=1}^{n} n_{ELPI+(p,v)} \cdot \Delta S_i\right)\frac{A_{nodal}}{A_{pin}} \quad (1)$$

$$\Delta S_i = v_i \Delta t + \frac{1}{2} a \Delta t^2 \quad (2)$$

where φ_{POD} denotes the sampling efficiency in the pin-on-disc experiment, $n_{ELPI+(p,v)}$ refers to the mass rate of airborne particles, which can be obtained via *pv*-map, A_{nodal} and A_{pin} are the element area in the brake pad and pin area, respectively, and ΔS_i refers to the sliding distance during a sub-step, which can be computed using linear motion equation (2). The sampling efficiency of brake wear PM_{10} emissions in the pin-on-disc experiment was determined to be 80.1% according to results of computational fluid dynamics performed by Riva et al. (2017).

2.2. Validation of simulation model

The WLTP-Brake cycle was developed based on the 700,000 vehicle driving data from Europe, the United States, India, Korea, and Japan (Woo et al., 2021), which already includes urban, rural, and motorway driving data. Thus, 303 samples from brake events of the WLTP-Brake cycle were collected on the brake dynamometer and used to validate the simulated results. The particle counter with an electric low-pressure impactor (ELPI+) was employed to measure particle emissions in the 0.004–10 μm range under WLTP-Brake on the brake dynamometer, and the measured particles were assumed to have a density of 1 g/cm^3 (Riva et al., 2019). The PM_{10} emissions per braking event were calculated based on the measured results, which were used to validate the FEA simulation approach. The experimental setup, which primarily included the brake dynamometer, wind tunnel, and particle counter, is illustrated in Fig. 5, in which the overall brake system was sealed inside an oval chamber. Clean air was supplied through high-efficiency particulate air filters (HEPA H13) to maintain a particle-free environment inside the oval chamber. The air combined with brake wear particles exited from the oval chamber into a 3.5-m-long, 150-mm-diameter wind tunnel. At the wind tunnel, a sample probe was attached. The brake wear particles were measured twice repeatedly on the brake dynamometer, and the maximum and average deviations of PM_{10} emissions throughout the WLTP-Brake driving cycle were determined to be roughly 27% and 15%, respectively.

The measured and simulated PM_{10} emissions were determined for the 303 braking events of the WLTP-Brake cycle. To further evaluate the

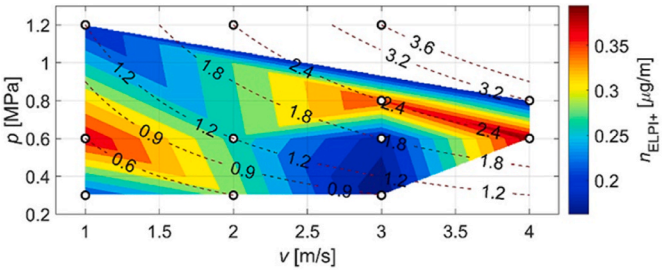

Fig. 4. The mass rate of the airborne particle (n_{ELPI+}) against sliding velocity (v) and normal contact pressure (p).

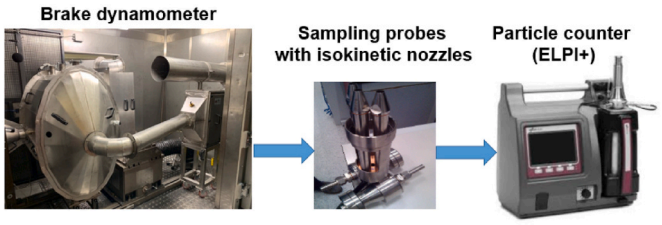

Fig. 5. Experimental setup used for measuring PM_{10} emissions.

performance of the FEA simulation approach, the square correlation coefficient (R^2) and root mean square error (*RMSE*) were calculated by the following equations:

$$R^2 = 1 - \frac{\sum (m_M - m_S)^2}{\sum (m_M - m_A)^2} \tag{3}$$

$$RMSE = \frac{1}{n}\sqrt{n\sum_{i=1}^{n}(m_{S_i} - m_{M_i})^2} \tag{4}$$

where m_{M_i} donates the measured PM_{10} emissions in i brake event throughout the WLTP-Brake driving cycle, m_{S_i} refers to the simulated PM_{10} emissions in i brake event, n refers to the total brake events throughout the WLTP-Brake driving cycle, and m_A is the average value of the measured PM_{10} emissions of 303 braking events. The results regarding R^2 and *RMSE* are shown in Fig. 6. As can be observed, the R^2 and RMSE were 0.93 and 0.018 mg, respectively, indicating that the proposed FEA approach can predict the PM_{10} emissions from brake wear. It means that the validated FEA approach is able to simulate the PM_{10} emissions from brake wear on various test driving cycles since the WLTP-Brake cycle already includes the urban, rural, and highway driving data. In this context, the brake wear PM_{10} emissions from 28 braking events from WLTP cycle and 215 braking events from LACT cycle were simulated using the validated FEA approach.

3. Results and discussion

3.1. Simulation of brake pad wear

Fig. 7 illustrates the distribution of FEA contact pressure on both sides of the piston and finger for three examples from WLTP, LACT, and WLTP-B cycles. These randomly selected examples corresponded to braking event #22 of the WLTP, LACT, and WLTP-B with the calliper cylinder pressures of 0.56 MPa, 0.42 MPa, and 0.39 MPa, respectively. The contour plots of the output simulation reflected the pressure distribution at the end of the braking events. As can be seen, the contours of

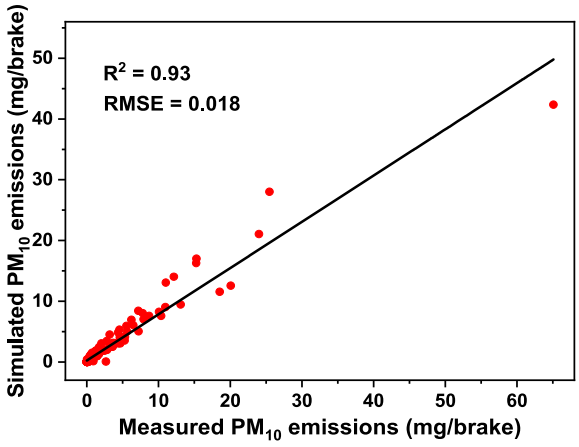

Fig. 6. Relationship between measured and simulated PM_{10} emissions under WLTP-Brake driving cycle.

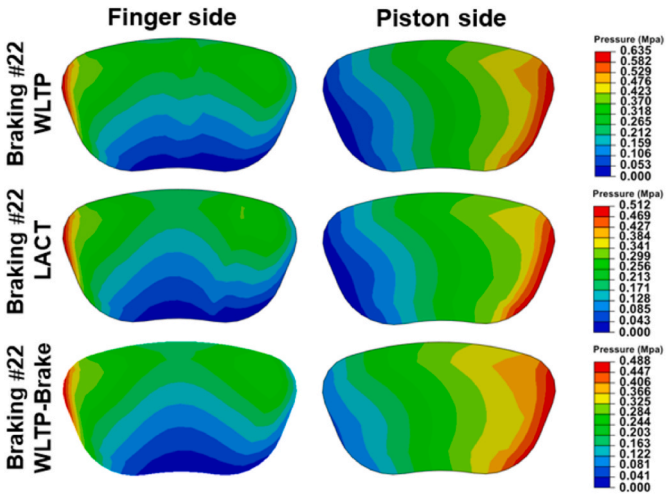

Fig. 7. Contour plots of contact pressure on both sides of the piston and finger for braking events #22 of WLTP, LACT, and WLTP-Brake. Arrows indicate the rotating direction of the brake rotor.

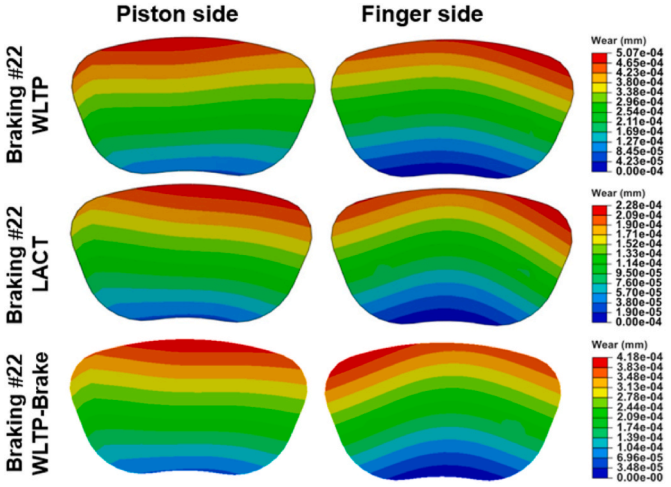

Fig. 8. Contour plots of pad wear on both sides of the piston and finger for the WLTP, LACT, and WLTP-B driving cycles. Arrows indicate the rotational direction of the brake rotor.

the three examples under various test driving cycles were similar. The contact pressure distribution on the finger side exhibited a gradient from low to higher radii, which was not substantially influenced by the braking conditions of the various test driving cycles. On the piston side, the contact pressure displayed a transversal gradient from the inner to the outer side. It is worth mentioning that the outer boundary of the piston pad under three test driving cycles showed higher pressure compared to the rest of the piston.

It can be seen from Fig. 7 that the contact pressure distributions on both sides of the piston and finger pads from the examples under three driving cycles were clearly distinct. Such a noticeable difference in contact pressure may be explained by the following causes:

- The load was applied in two different ways: the piston propelled one pad into contact with the brake disc, whilst the floating calliper forced the other pad into contact with the brake disc;
- Because the piston side pressure varied tangentially from the inner to the outer side, the brake torque generated by the revolving disc may only affect the piston side pad;

➢ The stable condition could not be achieved until the end of every braking event because the rotational velocity was always changing. As a result, there was no consistent distribution of contact pressure.

Similarly, AbuBakar and Ouyang (2008) used an FEA approach to evaluate the wear of friction material in a disc brake system and discovered that the contact pressure distributions on both pads of the piston and finger were significantly different. Recently, Riva et al. (2019) simulated brake wear during the LACT cycle using an FEA approach and found a significant distinction in contact pressure between the piston and finger side pads. In addition, Riva et al. (2020) simulated the friction coefficient of a brake system and observed different contact pressures on both sides of the piston and finger pads. However, the contour plots of contact pressure distribution obtained by Wahlström et al. (2009) differ from the results of our present work, probably because the effect of the floating calliper on contact pressure was not considered in their study. A previous study revealed that the floating calliper caused asymmetric impacts between both sides of the finger and piston pads (Riva et al., 2019).

Fig. 8 shows the corresponding contour plots of pad wear on both sides of the piston and finger for the braking events #22 under the WLTP, LACT, and WLTP-Brake cycles. Although the wear depth was different for braking events #22 of various test driving cycles, the pattern of contour plots of brake pad wear was similar. Compared to the piston pad side, the lower part of the finger pad exhibited less wear. Additionally, it can be observed that there was a gradient rise in pad wear on both sides from the inner to outer radii. This phenomenon is probably associated with the fact that external radii always have a greater sliding distance, which results in increased wear on both sides of the brake pads. Similarly, the FEA results performed by a previous study showed greater wear with the external radii of brake pads (Riva et al., 2019). In a study by Valota et al. (2017), they employed an FEA approach to compute the brake pad wear depth of the disc system equipped with a fixed calliper during the SAE-J2707 test cycle. The results showed that the pad wear was more homogeneous, but it was concentrated mostly in the upper section of the contact region, which is not in agreement with our results. Such a discrepancy is presumably connected with the following factors: 1) the test cycle was subdivided into blocks of equal deceleration braking in the literature, which was closer to the steady-state; 2) in comparison to the brake system with the fixed calliper in the literature, the contact pressure distribution for the brake system with the floating calliper may be different as their braking mechanisms differ. A previous study on a brake dynamometer has suggested that the PM generated from the braking system with the fixed calliper was up to 50% more than that with the floating calliper.

3.2. PM_{10} emissions under various test driving cycles

The speed profiles of the WLTP, LACT, and WLTP-Brake cycles and simulated PM_{10} emissions for every braking event of the three cycles obtained by the validated FEA approach are illustrated in Figs. 9–11. PM_{10} emissions for each braking event during various test-driving cycles were clearly different. It means that braking conditions affect brake wear PM_{10} emissions significantly. From Figs. 9–11, the brake wear PM_{10} emissions were apparent higher during high-speed braking applications, such as braking events #24 and #28 in the WLTP, braking events #66 and #69 in the LACT, and braking event #295 in the WLTP-Brake. This is likely caused by the intense deformation at the sliding surface, stemming from the high initial braking speed (see Figs. 9a, 10a and 11a) and larger deceleration rate (Park et al., 2021). During the WLTP cycle, the braking event #28 generated the highest PM_{10} emissions among the 28 braking events, braking from 123 km/h to 0 km/h with a deceleration of 1.14 m/s^2. In terms of the LACT cycle (see Fig. 10), the braking event with the most PM_{10} emissions was #65 which had the longest sliding distance, braking from 154 km/h to 36 km/h with a deceleration rate of 0.5 m/s^2. As shown in Fig. 11, the braking event #295 from 133 km/h to 34 km/h with a deceleration of 1.82 m/s^2 generated the most PM_{10} emissions throughout the WLTP-Brake cycle. From the braking conditions corresponding to the largest PM_{10} emissions during the three test driving cycles, it seems that the high initial braking speed and larger deceleration rate are probably the major causes of more PM_{10} emissions. A similar finding was reported by Park et al. (2021), who studied brake pad wear PM emissions during the WLTP cycle. They detected a substantial increase in brake wear PM emissions during high-speed braking operations and ascribed this to the intense deformation at the sliding surface. Woo et al. (2021) explored the brake wear particle emissions during various test driving cycles and discovered that the brake wear particles were a function of the brake energy

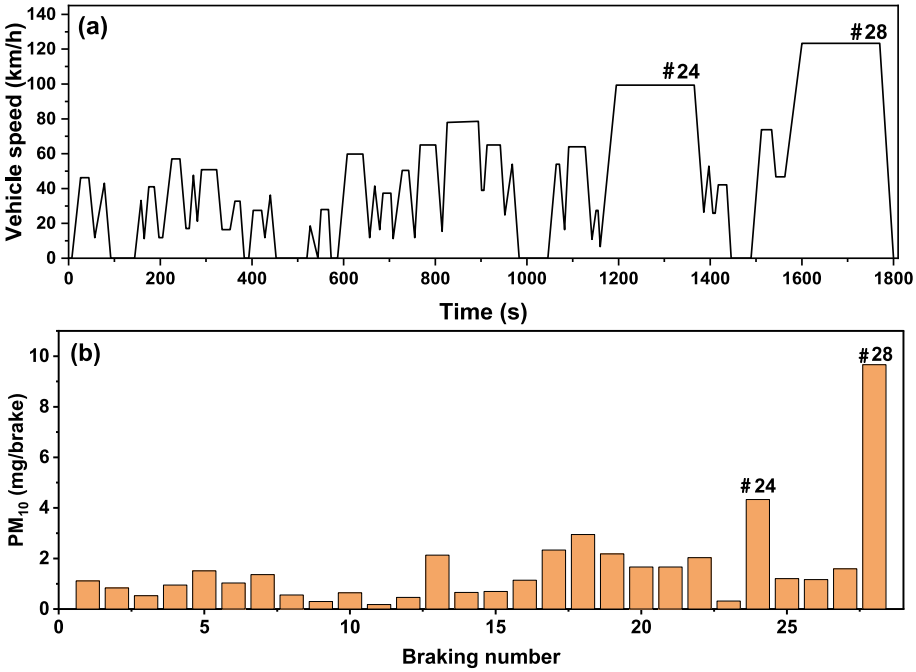

Fig. 9. Speed profile (a) and simulated PM_{10} emissions per braking event (b) during the WLTP cycle.

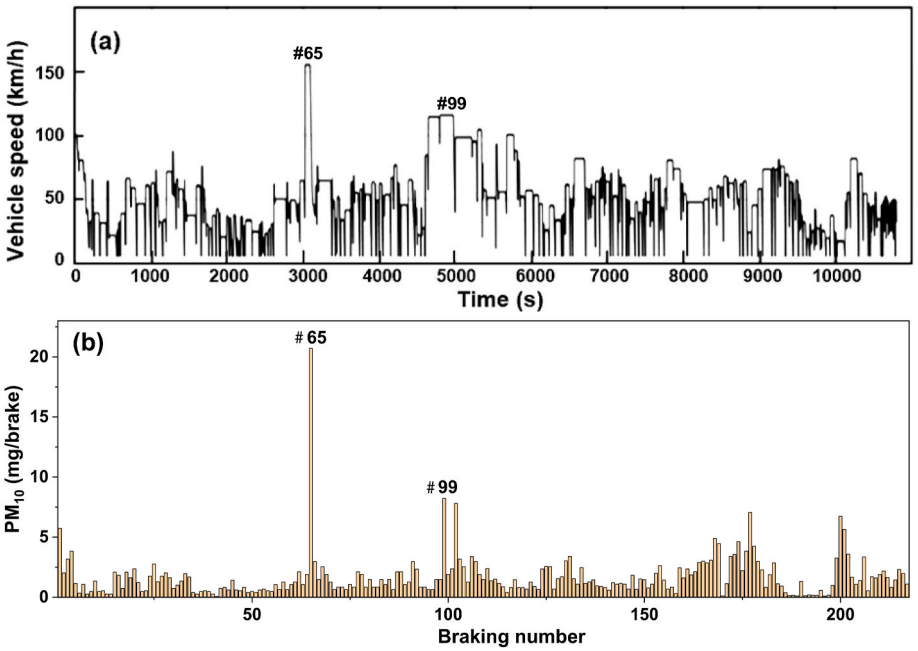

Fig. 10. Speed profile (a) and simulated PM_{10} emissions per braking event (b) during the LACT cycle.

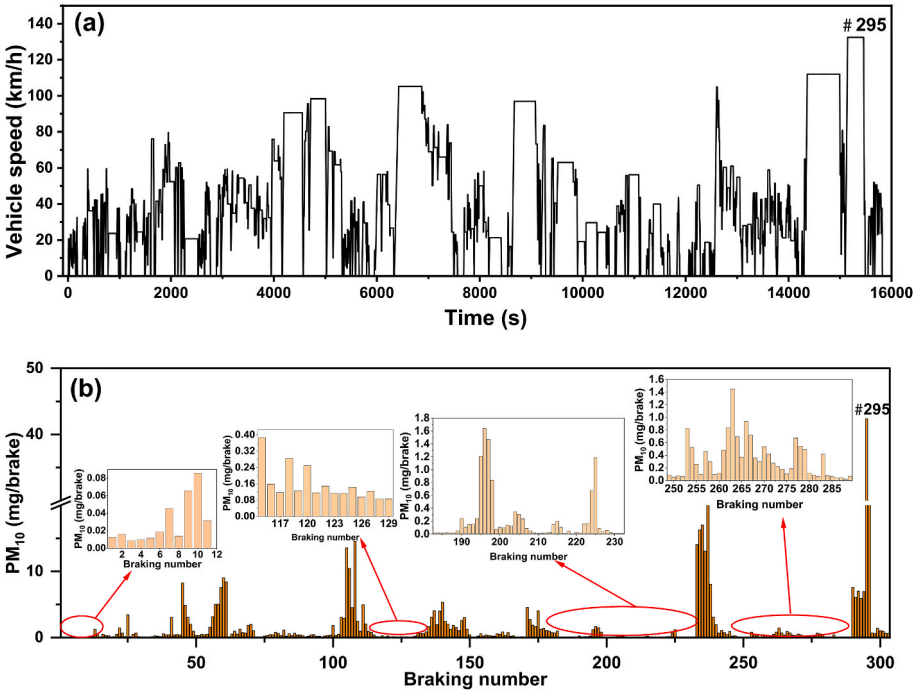

Fig. 11. Speed profile (a) and simulated PM_{10} emissions per braking event (b) during the WLTP-Brake cycle.

dissipated and initial braking speed during various test driving cycles. In addition, Zum Hagen et al. (2019) and Mathissen et al. (2018) found that high energy dissipated during braking would cause a substantial increase in the number of brake wear nanoparticles. From a thermodynamic standpoint, high energy dissipated during braking leads to an increase in the local temperature between the brake disc and pad friction surfaces, which results in the decomposition and volatilization of frictional material.

The emission factors were calculated on the basis of simulated PM_{10} emissions under three test driving cycles. The calculated results and relevant data from the literature are summarised in Table 1. The emission factors were 7.9 mg km^{-1} veh^{-1} for the WLTP, 9.8 mg km^{-1} veh^{-1} for the LACT, and 6.4 mg km^{-1} veh^{-1} for the WLTP-Brake. From Table 2, the LACT had the largest average deceleration rate, which may lead to a higher PM_{10} emission factor than the other two driving cycles. The average deceleration rate of the WLTP-Brake was higher than that of the WLTP, but the brake wear emission factor of the WLTP-Brake was lower. This meant that the brake wear PM_{10} emission factor was likely to be influenced not only by the braking deceleration rate, but also by other factors, such as braking frequency, braking duration, and initial braking speed. This finding is in agreement with the conclusion reported by Woo et al. (2021) and Hagen et al. (2019), who revealed that a variety of

Table 1
Summary of the PM_{10} emission factors (EFs) from brake wear.

PM_{10} EFs (mg km^{-1} veh^{-1})	Method	Reference
7.9	Simulation study	Present work (WLTP)
9.8	Simulation study	Present work (LACT)
6.4	Simulation study	Present work (WLTP-Brake)
6.2	Receptor modelling	Beddows and Harrison (2021)
7.4	Receptor modelling	Piscitello et al. (2021)
9.3	Receptor modelling	Timmers and Achten (2016)
7.4	Receptor modelling	Dahl et al. (2006)
5.8	Brake dynamometer study	Iijima et al. (2008)
8.1	Brake dynamometer study	Sanders et al. (2003)
5.2	Brake dynamometer study	Garg et al. (2000)
7.4	Emission inventory	EEA (2019)
7.0	Emission inventory	NAEI (2018)

Table 2
Braking characteristics under three test driving cycles.

Name abbreviation	WLTP	LACT	WLTP-Brake
Test time (min)	30	180	264
Driving distance (km)	23	150	192
Number of braking	28	217	303
Braking frequency (stop/km)	1.22	1.45	1.60
Average braking speed (km/h)	32.5	36.7	43.7
Average deceleration rate (m/s^2)	0.94 (range: 0.31–1.47)	1.07 (range: 0.20–2.88)	0.97 (range: 0.49–2.18)
Dissipation energy per distance (kJ/km)	203	210	126

factors, including initial braking speed, braking frequency and duration, influence the generation of brake wear particles, which can be assessed by the total dissipation energy. From Table 1, the obtained values of emission factors for three test driving cycles were consistent with the results reported in the literature. For example, the PM_{10} emission factors from brake wear were calculated to be in the range of 6.2–9.3 mg km^{-1} veh^{-1} using receptor modelling (Beddows and Harrison, 2021; Dahl et al., 2006; Piscitello et al., 2021; Timmers and Achten, 2016). In a brake dynamometer study by Sanders et al. (2003) and Iijima et al. (2008), they found PM_{10} emission factors of 8.1 mg km^{-1} veh^{-1} and 5.8 mg km^{-1} veh^{-1}, respectively. The PM_{10} emission factors were 7.4 mg km^{-1} veh^{-1} and 7.0 mg km^{-1} veh^{-1} according to the emission inventory (EEA, 2019; NAEI, 2018).

Fig. 12 illustrates the comparison of emission factors for PM_{10} and total wear mass generated from brake wear during three test driving cycles. It can be seen that the PM_{10} emission factor was the highest under the LACT, followed by the WLTP and WLTP-Brake. From Table 2, the LACT had a higher braking frequency and the highest average deceleration rate than the other two test driving cycles, which may be associated with the highest PM_{10} emissions. Compared to the WLTP and WLTP-Brake, the LACT corresponded mainly to the urban driving conditions, which generated more PM_{10} emissions. Similar findings were reported by Beddows and Harrison (2021) and Liu et al. (2021, 2022a), who used receptor modelling to evaluate the brake wear $PM_{2.5}$ and PM_{10} emissions on urban, rural and motorway roads. They found that both $PM_{2.5}$ and PM_{10} from brake wear on urban roads were apparently larger than those on rural and motorway roads. The PM_{10} emission factor under the WLTP, LACT and WLTP-Brake accounted for 40%, 43% and 36% of the overall emission factor of brake pad wear mass, respectively. This means that the test driving cycles had an effect on the generation of

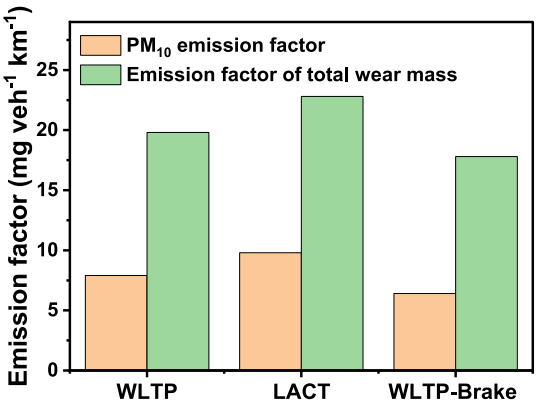

Fig. 12. Emission factors of PM_{10} and total brake wear mass during three test driving cycles.

PM_{10} emissions. These results are consistent with the data reported in most literature. For instance, Garg et al. (2000) reported that 10%–48% of total brake wear mass was distributed in PM_{10} fraction under various braking cases. Zum Hagen et al. (2019) used the cascade impactor and the Dusttrak (TSI 3090) to study the brake wear particles generated by the LACT driving cycle on the brake dynamometer, respectively. They found that utilizing these two devices, average PM_{10} emissions represented 49% and 40% of the overall brake weight loss, respectively. Hagino et al. (2016) discovered that brake wear PM_{10} accounted for around 32% of the total mass of brake wear. Riva et al. (2019) used the experimental and simulated approach to explore the brake wear emissions and revealed that 37% and 26% of total brake pad wear mass were PM_{10} emissions. However, Sanders et al. (2003) found that average brake wear PM_{10} mass accounted for up to 82% of total wear mass on the brake dynamometer test, which is probably related to the materials used in the brake pad.

4. Conclusions

This work focuses on the PM_{10} emissions generated from the brake wear of a passenger car per braking event during three test driving cycles (WLTP, LACT, and WLTP-Brake) using an FEA approach. Moreover, an electrical low-pressure impactor (ELPI+) was used to measure the PM_{10} emissions per braking event during the WLTP-Brake cycle on a brake dynamometer sealed in a chamber to validate a proposed FEA simulation approach. The simulated and experimental results with an R^2 value of 0.93 indicated that the proposed FEA simulation approach has the capacity to predict PM_{10} emissions from brake wear. A gradient increase in brake pad wear for the FEA data was observed from the inner to outer radii. The simulated PM_{10} emission factors were 7.9 mg km^{-1} veh^{-1}, 9.8 mg km^{-1} veh^{-1}, and 6.4 mg km^{-1} veh^{-1}, respectively, for the WLTP, LACT, and WLTP-Brake. The LACT cycle had the highest ratio of emission factors for PM_{10} to total brake wear mass, followed by the WLTP and WLTP-Brake cycles. In practice, lowering the frequency of high-speed braking may be an efficient strategy to reduce PM_{10} emissions. It is worth mentioning that only simulated PM_{10} emission factors were determined under various test driving cycles, whilst the simulated $PM_{2.5}$ emission factors were not evaluated in the present work. Further work is required to calculate the $PM_{2.5}$ emission factors under different test driving cycles when a *pv*-map of the $PM_{2.5}$ mass rate is available. In addition, the number of airborne particles is needed from brake wear using the similar FEA approach.

Author contributions statement

Ye Liu: Investigation, Methodology, Data visualisation, Writing-original draft. **Haibo Chen**: Conceptualisation, Funding acquisition, Project administration. **Chuhan Yin**: Software, Writing-review &

editing. **Matteo Federic**: Resources, Data curation; Writing-review & editing. **Guido Perricone**: Resources, Data curation. **Ying Li**: Methodology, Writing-review & editing. **Dimitris Margaritis**: Writing-review & editing. **Yang Shen:** Software, Data curation, Writing-review & editing. **Junhua Guo:** Writing-review & editing. **Tangjian Wei:** Investigation, Writing-review & editing.

Declaration of competing interest

The authors declare that they have no known competing financial interests or personal relationships that could have appeared to influence the work reported in this paper.

Data availability

Data will be made available on request.

Acknowledgments

This research was supported by the European Union's Horizon 2020 research and innovation programme: MODALES (grant agreement No 815189, https://modales-project.eu/) aimed at modifying drivers' behaviour to reduce vehicle emissions from brake wear.

References

ABAQUS, 2014. Information of Abaqus ALE Technique available at: http://abaqus.software-re.polimi.it/v6.14/books/usi/default.htm?startat=pt03ch14s06.html.
AbuBakar, A.R., Ouyang, H., 2008. Wear prediction of friction material and brake squeal using the finite element method. Wear 264 (11–12), 1069–1076.
Beddows, D.C.S., Harrison, R.M., 2021. PM10 and PM2.5 emission factors for non-exhaust particles from road vehicles: dependence upon vehicle mass and implications for battery electric vehicles. Atmos. Environ. 244.
Contardo, T., Vannini, A., Sharma, K., Giordani, P., Loppi, S., 2020. Disentangling sources of trace element air pollution in complex urban areas by lichen biomonitoring. A case study in Milan (Italy). Chemosphere 256, 127155.
Dahl, A., Gharibi, A., Swietlicki, E., Gudmundsson, A., Bohgard, M., Ljungman, A., Blomqvist, G., Gustafsson, M., 2006. Traffic-generated emissions of ultrafine particles from pavement–tire interface. Atmos. Environ. 40 (7), 1314–1323.
EEA, 2018. European Union Emission Inventory Report 1990-2016 under the UNECE Convention on Long-Range Transboundary Air Pollution (LRTAP). EEA Report.
EEA, 2019. Airbase - the European Air Quality Database. European Environment Agency.
Garg, B.D., Cadle, S.H., Mulawa, P.A., Groblicki, P.J., Laroo, C., Parr, G.A., 2000. Brake wear particulate matter emissions. Environ. Sci. Technol. 34 (21), 4463–4469.
Gasser, M., Riediker, M., Mueller, L., Perrenoud, A., Blank, F., Gehr, P., Rothen-Rutishauser, B., 2009. Toxic effects of brake wear particles on epithelial lung cells in vitro. Part. Fibre Toxicol. 6 (1), 1–13.
Grigoratos, T., Martini, G., 2015. Brake wear particle emissions: a review. Environ. Sci. Pollut. Control Ser. 22 (4), 2491–2504.
Hagen, F.H.F., Mathissen, M., Grabiec, T., Hennicke, T., Rettig, M., Grochowicz, J., Vogt, R., Benter, T., 2019. On-road vehicle measurements of brake wear particle emissions. Atmos. Environ. 217, 116943.
Hagino, H., Oyama, M., Sasaki, S., 2015. Airborne brake wear particle emission due to braking and accelerating. Wear 334, 44–48.
Hagino, H., Oyama, M., Sasaki, S., 2016. Laboratory testing of airborne brake wear particle emissions using a dynamometer system under urban city driving cycles. Atmos. Environ. 131, 269–278.
Harrison, R.M., Jones, A.M., Gietl, J., Yin, J., Green, D.C., 2012. Estimation of the contributions of brake dust, tire wear, and resuspension to nonexhaust traffic particles derived from atmospheric measurements. Environ. Sci. Technol. 46 (12), 6523–6529.
Iijima, A., Sato, K., Yano, K., Kato, M., Kozawa, K., Furuta, N., technology, 2008. Emission factor for antimony in brake abrasion dusts as one of the major atmospheric antimony sources. Environ. Sci. Technol. 42 (8), 2937–2942.
Klöckner, P., Seiwert, B., Weyrauch, S., Escher, B.I., Reemtsma, T., Wagner, S., 2021. Comprehensive characterization of tire and road wear particles in highway tunnel road dust by use of size and density fractionation. Chemosphere 279, 130530.
Kukutschová, J., Moravec, P., Tomášek, V., Matějka, V., Smolík, J., Schwarz, J., Seidlerová, J., Šafářová, K., Filip, P., 2011. On airborne nano/micro-sized wear particles released from low-metallic automotive brakes. Environ. Pollut. 159 (4), 998–1006.
Lawrence, S., Sokhi, R., Ravindra, K., Mao, H., Prain, H.D., Bull, I.D., 2013. Source apportionment of traffic emissions of particulate matter using tunnel measurements. Atmos. Environ. 77, 548–557.
Liu, Y., Chen, H., Gao, J., Li, Y., Dave, K., Chen, J., Federici, M., Perricone, G., 2021. Comparative analysis of non-exhaust airborne particles from electric and internal combustion engine vehicles. J. Hazard Mater. 420, 126626.
Liu, Y., Chen, H., Li, Y., Gao, J., Dave, K., Chen, J., Li, T., Tu, R., 2022a. Exhaust and non-exhaust emissions from conventional and electric vehicles: a comparison of monetary impact values. J. Clean. Prod. 331, 129965.
Liu, Y., Song, C., Lv, G., Cao, X., Wang, L., Qiao, Y., Yang, X., 2016. Surface functional groups and sp 3/sp 2 hybridization ratios of in-cylinder soot from a diesel engine fueled with n -heptane and n -heptane/toluene. Fuel 179, 108–113.
Liu, Y., Zhang, X., Lyu, G., Qiao, Y., Zhang, W., Song, C., 2022b. Effect of the oxidation-induced fragmentation of primary particles on soot oxidation reactivity. Combust. Flame 240.
Mathissen, M., Evans, C., 2019. Lowbrasys brake wear cycle-3h LACT. Mendeley Data 1.
Mathissen, M., Grochowicz, J., Schmidt, C., Vogt, R., Farwick zum Hagen, F.H., Grabiec, T., Steven, H., Grigoratos, T., 2018. A novel real-world braking cycle for studying brake wear particle emissions. Wear 414–415, 219–226.
NAEI, 2018. Road Transport Emission Factor from NAEI 2018. https://naei.beis.gov.uk/data/ef-transport.
Pant, P., Harrison, R.M., 2013. Estimation of the contribution of road traffic emissions to particulate matter concentrations from field measurements: a review. Atmos. Environ. 77, 78–97.
Park, J., Joo, B., Seo, H., Song, W., Lee, J.J., Lee, W.K., Jang, H., 2021. Analysis of wear induced particle emissions from brake pads during the worldwide harmonized light vehicles test procedure (WLTP). Wear 466–467.
Piscitello, A., Bianco, C., Casasso, A., Sethi, R., 2021. Non-exhaust traffic emissions: sources, characterization, and mitigation measures. Sci. Total Environ. 766, 144440.
Riva, G., Valota, G., Perricone, G., Wahlström, J., 2019. An FEA approach to simulate disc brake wear and airborne particle emissions. Tribol. Int. 138, 90–98.
Riva, G., Varriale, F., Wahlström, J., 2020. A finite element analysis (FEA) approach to simulate the coefficient of friction of a brake system starting from material friction characterization. Friction 9 (1), 191–200.
Riva, G., Wahlström, J., Alemani, M., Olofsson, U., 2017. In: A CFD Study of a Pin-On-Disc Tribometer Setup Focusing on Airborne Particle Sampling Efficiency, ECOTRIB 2017, 6th European Conference on TRIBology 7–9 June 2017. Ljubljana, Slovenia.
Sanders, P.G., Xu, N., Dalka, T.M., Maricq, M.M., 2003. Airborne brake wear debris: size distributions, composition, and a comparison of dynamometer and vehicle tests. Environ. Sci. Technol. 37 (18), 4060–4069.
Schmidt, A.A., Schmidt, T., Grabherr, O., Bartel, D., 2018. Transient wear simulation based on three-dimensional finite element analysis for a dry running tilted shaft-bushing bearing. Wear 408, 171–179.
Shupert, L.A., Ebbs, S.D., Lawrence, J., Gibson, D.J., Filip, P., 2013. Dissolution of copper and iron from automotive brake pad wear debris enhances growth and accumulation by the invasive macrophyte Salvinia molesta Mitchell. Chemosphere 92 (1), 45–51.
Timmers, V.R.J.H., Achten, P.A.J., 2016. Non-exhaust PM emissions from electric vehicles. Atmos. Environ. 134, 10–17.
Tutuianu, M., Bonnel, P., Ciuffo, B., Haniu, T., Ichikawa, N., Marotta, A., Pavlovic, J., Steven, H., 2015. Development of the World-wide harmonized Light duty Test Cycle (WLTC) and a possible pathway for its introduction in the European legislation. Transport. Res. Transport Environ. 40, 61–75.
Valota, G., De Luca, S., Söderberg, A., 2017. Using a Finite Element Analysis to Simulate the Wear in Disc Brakes during a Dyno Bench Test Cycle. Proceedings of the Eurobrake, pp. 2–4. Dresden, Germany.
Wahlström, J., Matejka, V., Lyu, Y., Söderberg, A., 2017. Contact pressure and sliding velocity maps of the friction, wear and emission from a low-metallic/cast-Iron disc brake contact pair. Tribol. Indust. 39 (4), 460–470.
Wahlström, J., Söderberg, A., Olofsson, U., 2009. Simulation of Airborne Wear Particles from Disc Brakes. SAE Technical Paper.
Woo, S.-H., Kim, Y., Lee, S., Choi, Y., Lee, S., 2021. Characteristics of brake wear particle (BWP) emissions under various test driving cycles. Wear 480–481.
Zhang, J., Zhang, X., Wu, L., Wang, T., Zhao, J., Zhang, Y., Men, Z., Mao, H., 2018. Occurrence of benzothiazole and its derivates in tire wear, road dust, and roadside soil. Chemosphere 201, 310–317.
Zhang, W., Song, C., Lyu, G., Bi, F., Wang, T., Liu, Y., Qiao, Y., 2021. Petroleum and Fischer–Tropsch diesel soot: a comparison of morphology, nanostructure and oxidation reactivity. Fuel 283.
Zum Hagen, F.H.F., Mathissen, M., Grabiec, T., Hennicke, T., Rettig, M., Grochowicz, J., Vogt, R., Benter, T., 2019. Study of brake wear particle emissions: impact of braking and cruising conditions. Environ. Sci. Technol. 53 (9), 5143–5150.